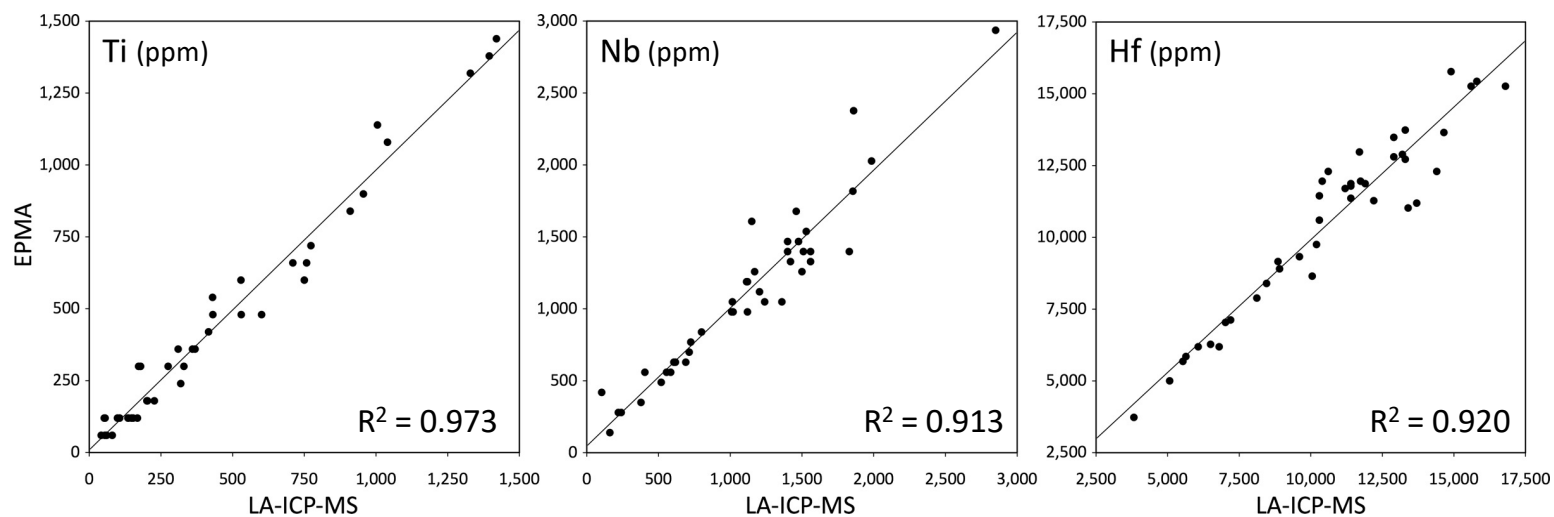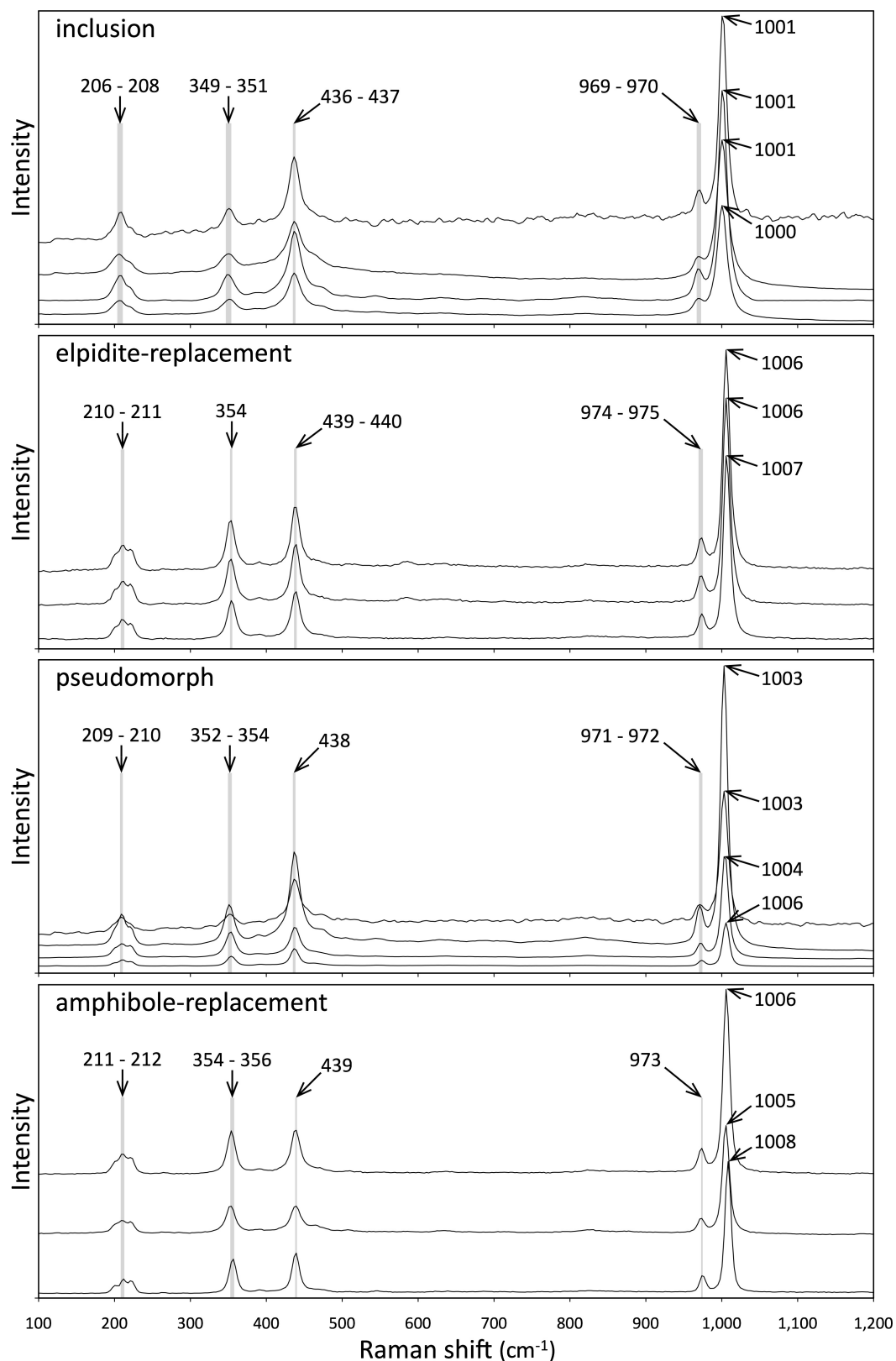# Appendix 3


Appendix 3. EPMA vs. LA-ICP-MS for Ti, Nb, and Hf concentrations in the metasomatic zircon from the agpaitic granite at Baerzhe, showing the correlation trends between the two methods. R^2 is the best fit to the trend.
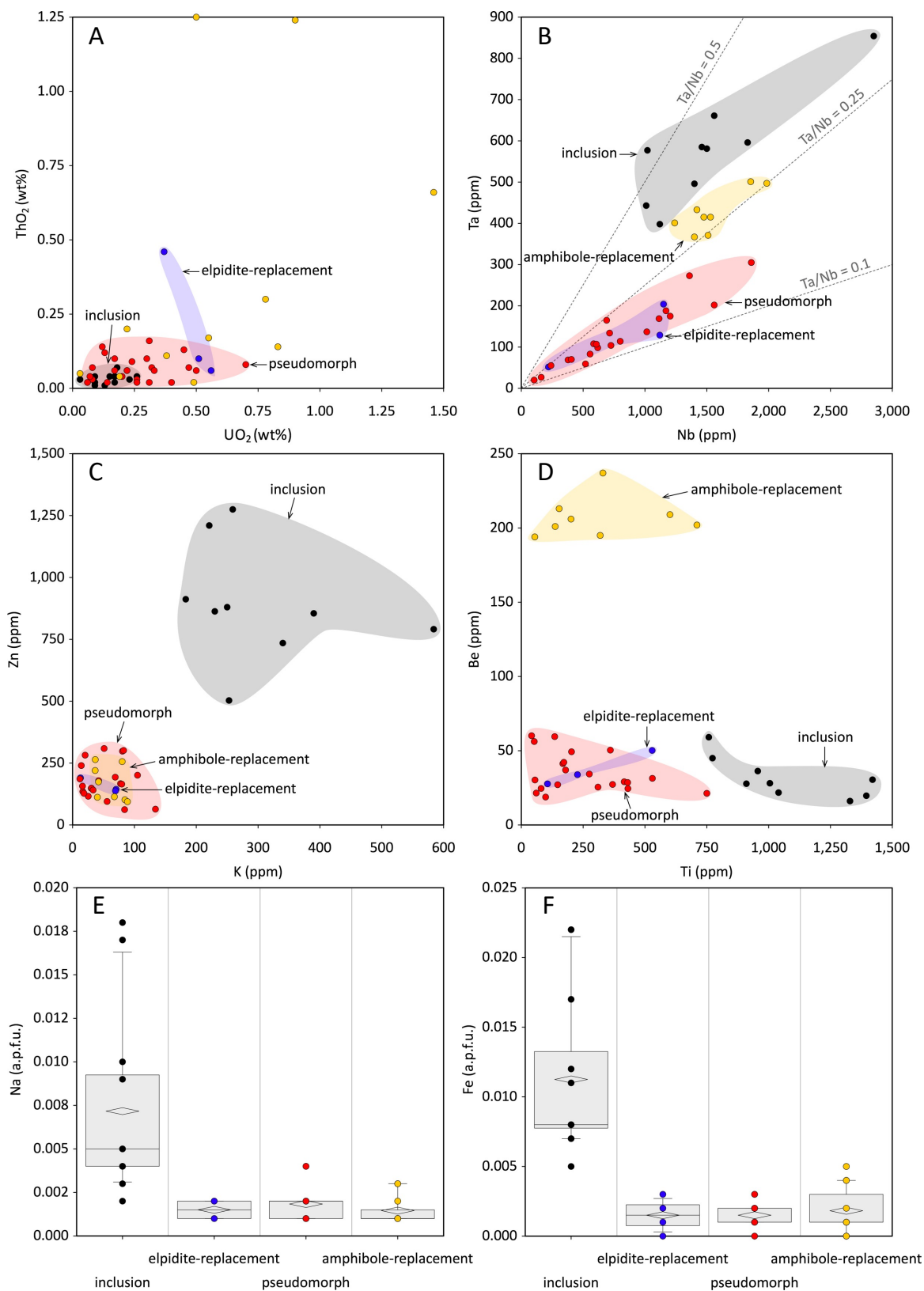
Appendix 4

Appendix 4. Representative Raman spectra of the different types of metasomatic zircon examined in this study. The five most evident Raman bands of these metasomatic zircon types in the agpaitic granite are 206 – 212, 349 – 356, 436 – 440, 969 – 975, and 1,000 – 1,008 cm^{-1}.The inclusion zircon exhibits the lowest values in all five bands (cf. Appendix 5).
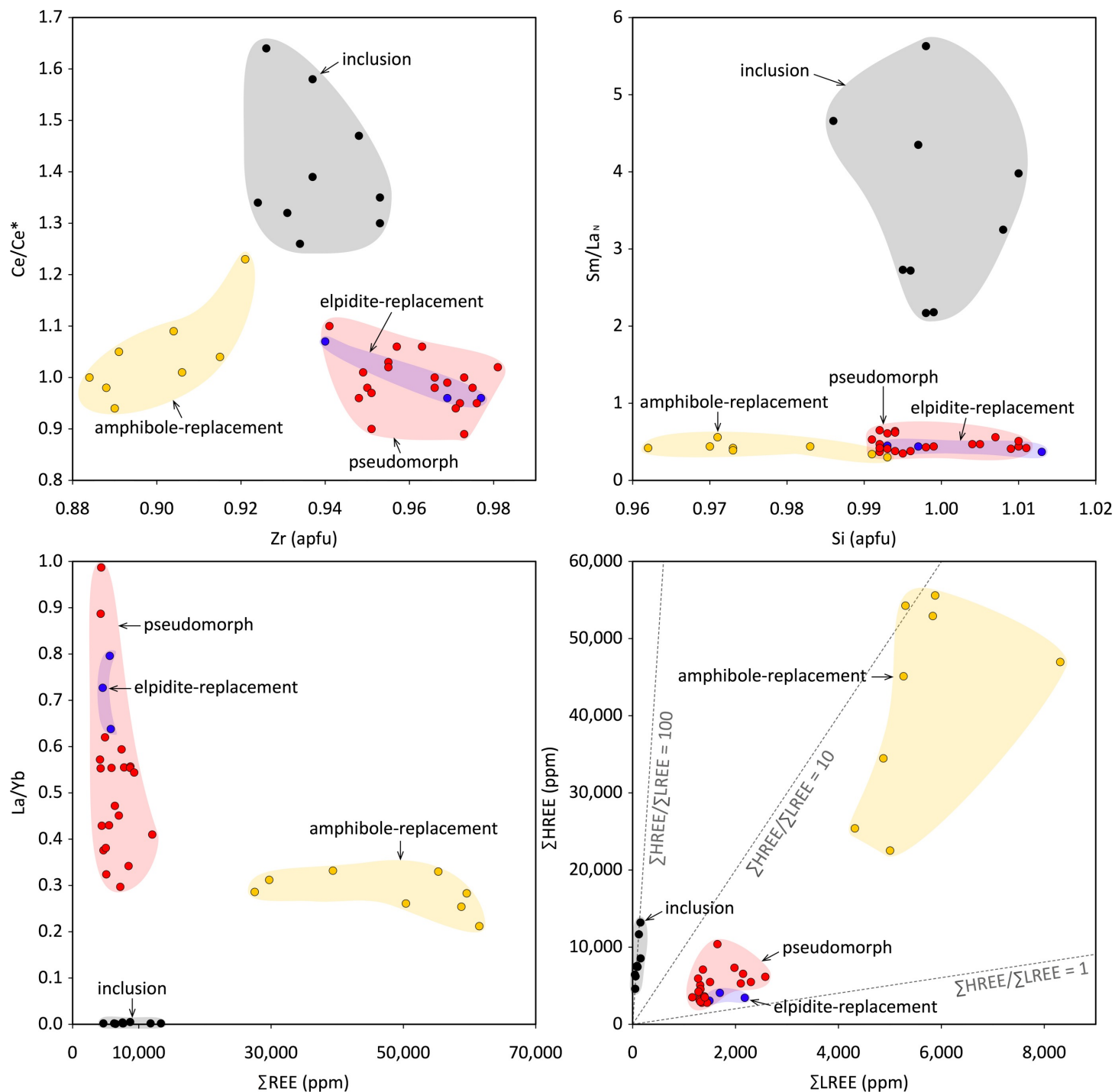
Appendix 5
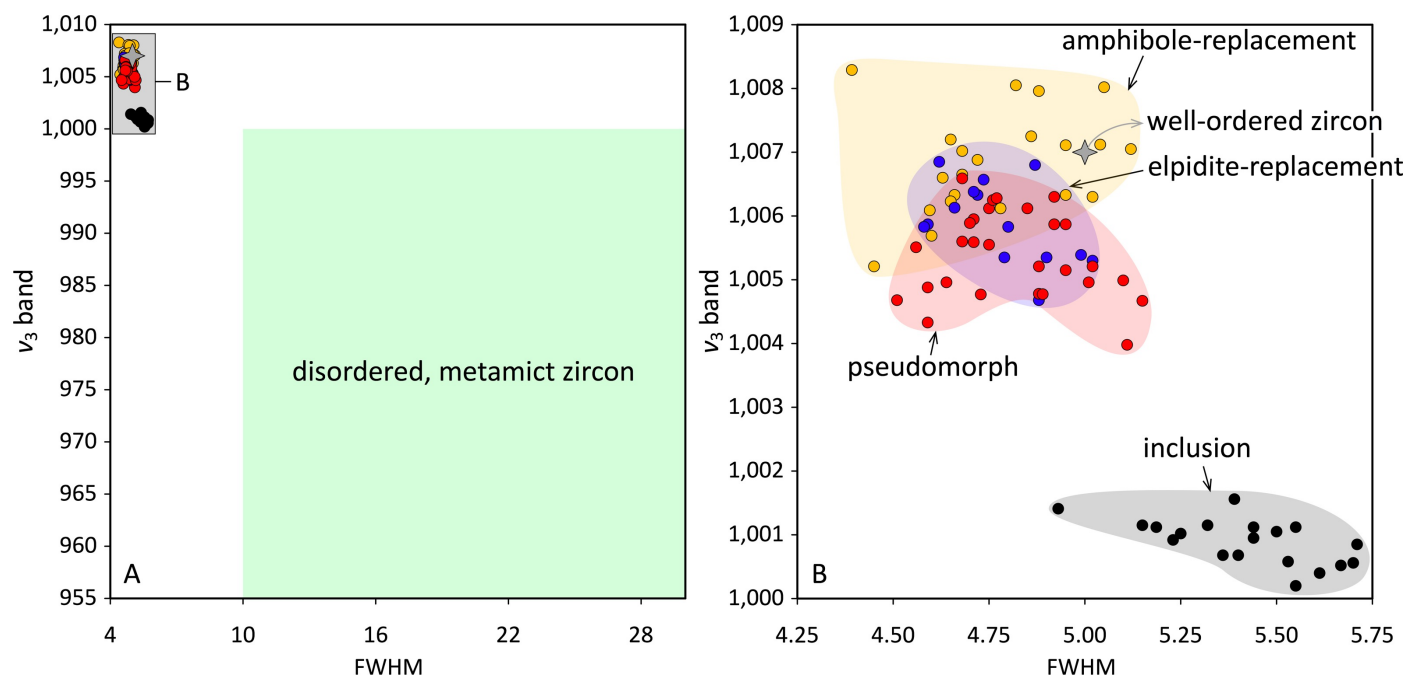
Appendix 5. The v_3 band positions vs. full-width at half-maximum (FWHM) values of representative Raman spot analyses of the different types of metasomatic zircon in the agpaitic granite at Baerzhe. The values and ranges for well-ordered and disordered zircon are from Nasdala et al. (2001) and Resentini et al. (2020).
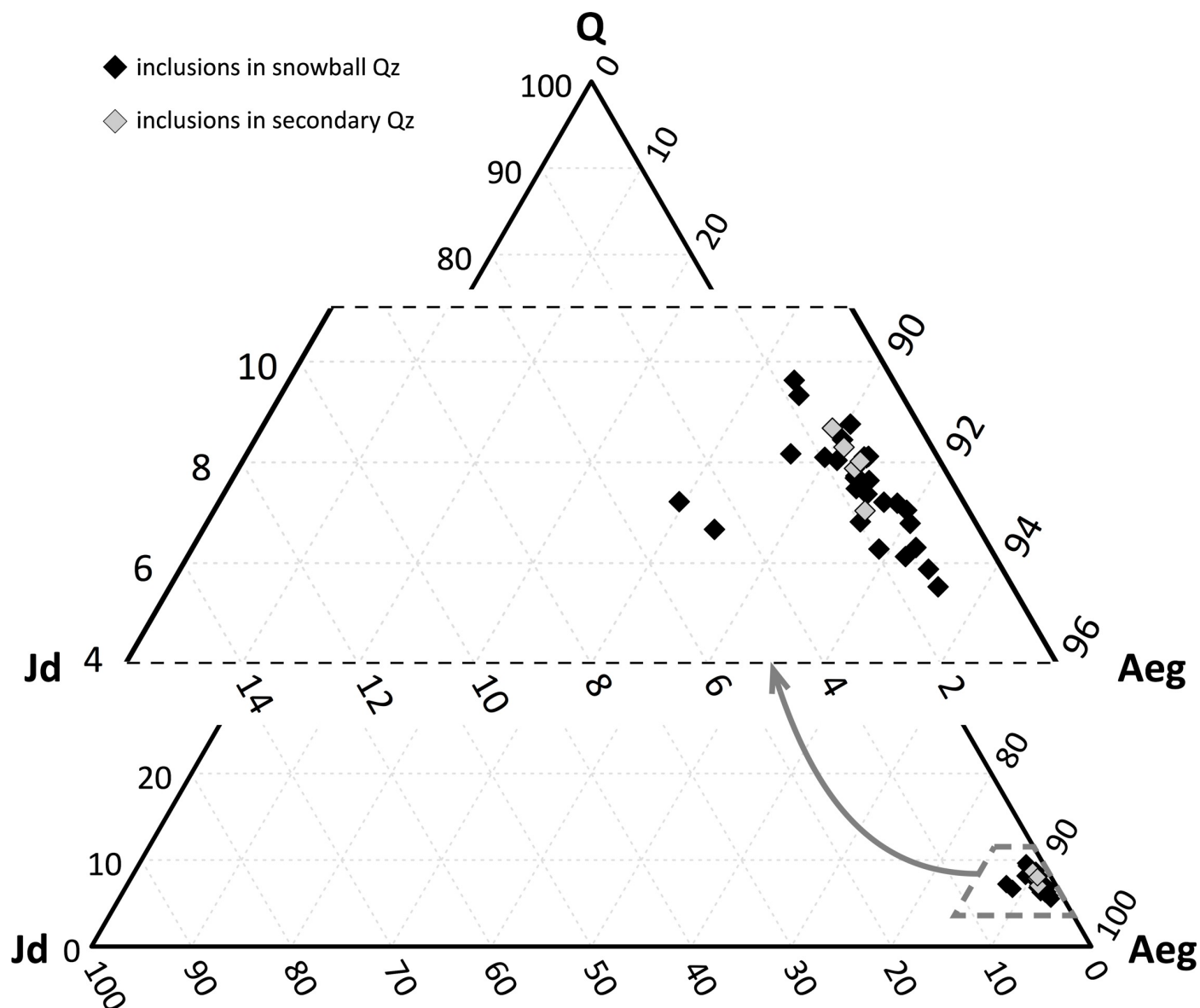
Appendix 6

Appendix 6. Bivariate plots and box-whisker diagrams that illustrate the representative chemical features of the four types of metasomatic zircon. These plots demonstrate that the inclusion and amphibole-replacement zircon are chemically distinct, whereas the pseudomorph and elpidite-replacement zircon are chemically similar and constitute a separate population from the inclusion and amphibole-replacement zircon. (A) ThO_2 vs. UO_2 concentration. (B) Ta vs. Nb concentration. Ta/Nb values of 0.1, 0.25, and 0.5 are indicated as dashed grey lines. (C) Zn vs. K concentration. (D) Be vs. Ti concentration. (E, F) Relative concentrations of Na and Fe (in a.p.f.u.) showing that the inclusion zircon contains the highest concentrations of these two elements among the four types.
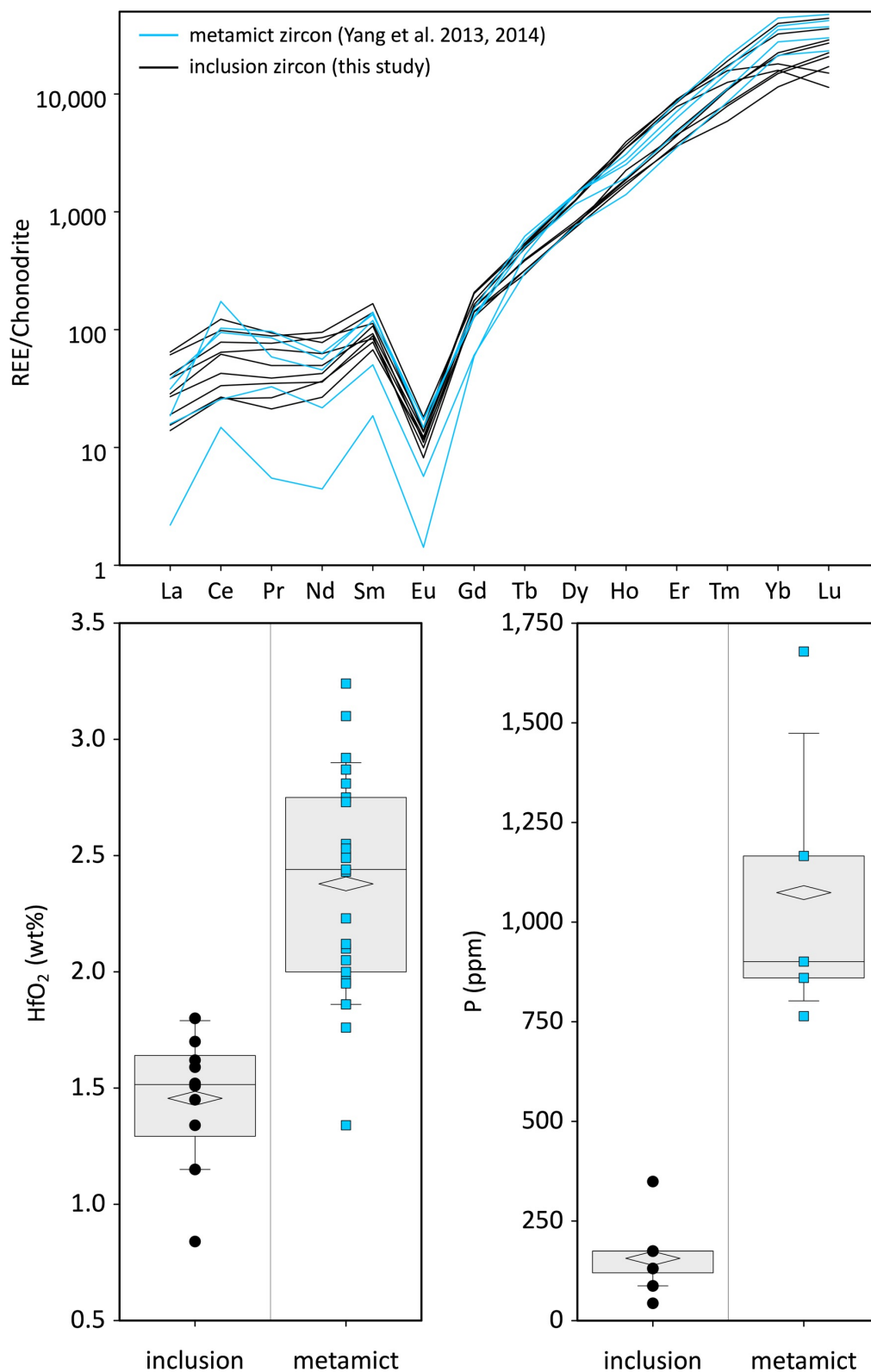
Appendix 7

Appendix 7. Bivariate plots showing key aspects of the REE chemistry of the metasomatic zircon. Three populations are evident, represented by the pseudomorph/elpidite-replacement zircon, the inclusion zircon, and the amphibole-replacement zircon. ΣHREE/ΣLREE values of 1, 10, and 100 are indicated as dashed grey lines. Ce/Ce* = $(Ce_N/(La_N \times Pr_N)^{1/2})$ and Sm/La $_N$ = (Sm_N/La_N), where N denotes chondrite-normalized values.

Appendix 8

Appendix 8. Ternary classification diagram for Ca-Na and Na pyroxenes in terms of the end-members Jadeite (Jd), Aegirine (Aeg), and Q (the sum of enstatite, ferrosilite, diopside, hedenbergite compoenents), modified after Morimoto et al. (1988). These data show that the aegirine inclusions in snowball and secondary quartz from Baerzhe are comparable in composition, and close to the end-member composition of aegirine.

Appendix 9

Appendix 9. Comparison of the chondrite-normalized REE distributions and the Hf and P concentration of the metamict zircon reported by Yang et al. (2013, 2014) and the inclusion zircon examined in this study.